Two-color nonlinear Boltzmann cellular automata: Surface tension and wetting

U. D'Ortona and D. Salin

*Laboratoire d'Acoustique et Optique de la Matière Condensée, Université Pierre et Marie Curie,
75252 Paris, France
and Laboratoire Fluides Automatique et Systémes Thermiques, Batiment 502, Campus Universitaire,
91405 Orsay Cedex, France*

Marek Cieplak

Institute of Physics, Polish Academy of Sciences, 02-668 Warsaw, Poland

Renata B. Rybka

*Institute of Geophysics, Department of Physics of Atmospheres, Polish Academy of Sciences,
01-452 Warsaw, Poland*

Jayanth R. Banavar

*Department of Physics and Materials Research Laboratory, Pennsylvania State University, 104 Davey Laboratory,
University Park, Pennsylvania 16802*

We have designed and tested a two-color nonlinear Boltzmann cellular automaton to study hydrodynamic phenomena related to surface tension and wetting in two dimensions. Our rules for collisions of colored particles allow for both miscibility and flexible control of the interfacial tension and the interface thickness. The contact angle of two fluids on a surface can be adjusted from complete wetting to complete nonwetting in a continuous way. Problems of the dynamical contact angle and drop deformation in a shear flow and in a gravitational field are also studied in detail.

PACS number(s): 02.70.Ns, 68.45.Gd, 05.50.+q, 47.11.+j

I. INTRODUCTION

Cellular automata (CA) models are used to facilitate generation of solutions to nonlinear partial differential equations [1,2]. These models are defined in terms of fictitious particles which move synchronously between sites of a regular lattice and undergo collisions on the sites of the lattice. The collision rules needed to simulate hydrodynamics should be chosen in a way that guarantees a microscopic conservation of mass and momentum and does not have spurious symmetries. Frisch, Hasslacher, and Pomeau [3] (FHP) have shown that such two-dimensional (2D) CA can be easily constructed and that the behavior characteristic of the 2D Navier-Stokes equations is imitated provided one considers triangular lattices and sufficient averaging over lattice cells is made. Similar methods to study 3D systems have also been developed [1,4].

The CA approach allows one to study many body phenomena in a toy kinetic model from which hydrodynamic behavior is readily obtained after simple coarse graining. The CA have been used to study two-fluid systems with interfaces [5], viscous fingers [6], systems undergoing the liquid-gas transition [7], suspensions [8], polymers [9], and phenomena of dispersion [10] and diffusion [11] and many other systems.

The CA used in fluid problems are usually of a Boolean nature: discrete velocity states at a site are either occupied or not, as in the original FHP model and its later generalizations. The magnitude of the velocity is usually equal to either 1 or 0. In the latter case we say that the particle is at rest. The occupation of this state is also Boolean. The particles are of a unit mass and are indistinguishable.

Recently, automata involving continuous degrees of freedom have been introduced [12–14]. The dynamics of these so called Boltzmann cellular automata (BCA) are defined in terms of flows of probabilities. In this case, ensembles of microscopic configurations are considered and the individual event collision rules correspond to one of the sets of rules used by FHP (e.g., FHP model II rules). Compared to the Boolean automata, the Boltzmann cellular automata require no coarse graining and the noise and equilibration times are reduced significantly.

A linearization of the probability distributions in BCA around their uniform steady state values is usually adopted to accelerate the computation [12–15] and has been used for the development of other efficient approaches [16]. While the linearization of the collision operator is satisfactory for a large class of problems, difficulties might arise in the study of situations which are far away from equilibrium.

We have developed another kind of two-dimensional BCA which has two additional features compared to the standard models: (a) the probability distributions are not linearized, i.e., the full nonlinear dynamics are considered, and (b) the collision rules can be modified to allow for many, n_0, particles at rest so that for selected values of n_0 and densities the system becomes Galilean

invariant. The two features (a) and (b) have been used separately in the literature on CA [12,13] before but we have put these two features together in one BCA system and then generalized it further to two-fluid systems to study interfaces.

We have employed the single fluid version of our BCA to study chaotic mixing [17] in rectangular [18] and circular [19] geometries. We have tested it in simple flows like Couette and Poiseuille, and studied its viscosity [19]. These studies dealt with single-fluid flows and this BCA system was found to be very useful and physically appropriate even when the boundaries of the system were complicated. The single-fluid system that we used in Refs. [16,17], has not yet been described in any detail so we present it here in Sec. II.

In this paper, however, our main focus is on two-fluid problems. We construct, in Sec. III, a nonlinear and Galilean-invariant two-fluid, or two-"color," BCA to study interfaces. Two-fluid interfaces should be characterized by a depletion of the density in their vicinity which arises due to an effective repulsion of the two fluids below the consolute point. The corresponding density profile is not uniform. We introduce a two-parameter control of the interface which allows for the coefficient of the surface tension and for the interface thickness to acquire wide ranges of values. In Sec. IV, we discuss the resulting properties of an interface between the two fluids. In Sec. V we consider droplet deformation in a shear flow.

We then focus on wetting phenomena. These phenomena have been thoroughly investigated in the past, both experimentally and theoretically [20–26], due to their great practical interest. Recently [21], the role of long range forces has been elucidated and has led to a coherent understanding of the spreading of liquid on a solid surface. This understanding of spreading dynamics is restricted to simple situations such as the motion of a drop on a flat surface. Real spreading is affected by surface roughness, chemical heterogeneity, mixed wettability [21], etc. Studying these complexities requires theoretical tools such as molecular dynamics [23–25], which, however, has limitations. The BCA, though less realistic, appears to be well suited to study such problems and we discuss the simplest applications of it in the remaining sections of the paper. In Sec. VI we introduce wetting properties by assigning color to walls and then study the static contact angle as a function of the relative color content of the wall. In Sec. VII we consider the effects of gravity on wetting, and finally in Sec. VIII we focus on wetting dynamics.

II. SINGLE-FLUID BOLTZMANN CELLULAR AUTOMATA

For convenience, let us introduce our BCA by first discussing the Boolean FHP cellular automata.

The FHP cellular automaton is defined on a triangular lattice [1,3]; at each site there are then seven allowed velocity states:

$$\vec{c}_0 = (0,0),$$

$$\vec{c}_\alpha = \left(\cos\left[\frac{\pi}{3}(\alpha - 1)\right], \sin\left[\frac{\pi}{3}(\alpha - 1)\right] \right),$$

$$\alpha = 1, \ldots, 6. \quad (1)$$

The state of the system is defined by the occupation numbers s_α (equal to 0 or 1) of these states at all sites. For the initial configuration, an average number of particles ρ_s is assigned at each site, or equivalently ρ particles per state (ρ will be referred to as the reduced density). Note that $\rho_s = (6 + n_0)\rho$ where n_0 is the maximum allowed number of rest particles at a site.

The cellular automaton updating rules consist of two steps, propagation and collision, each one occurring at each time step of the discrete time. The set of the chosen collision rules determines the viscosity of the system. For instance, in the so called model FHP II with $n_0 = 1$ the rules involve certain classes of binary, triple, and ternary collisions as described in Ref. [1]. The role of the triple collisions is to remove spurious symmetries which purely binary collisions would lead to. However, at low density the occurrence of such collisions is not frequent. Introducing particles at rest helps to remove the spurious symmetries and allows one to reduce average flow velocities. Ternary collisions make the roles of particles and holes symmetric.

The complete dynamics of the system is described by the evolution equation

$$s_\alpha(t + 1, \vec{r} + \vec{c_\alpha}) = s_\alpha(t, \vec{r}) + \mathcal{C}_\alpha(\{s_\alpha\}), \quad (2)$$

where $\vec{r}$ is a vector pointing at a node of the lattice and $\mathcal{C}_\alpha(\{s_\alpha\})$ is the collision operator. For example, the three-particle collision term is represented by

$$\mathcal{C}_\alpha^3 = s_{\alpha+1}s_{\alpha+3}s_{\alpha+5}(1 - s_{\alpha+2})(1 - s_{\alpha+4})(1 - s_{\alpha+6})$$
$$- s_\alpha s_{\alpha+2}s_{\alpha+4}(1 - s_{\alpha+1})(1 - s_{\alpha+3})(1 - s_{\alpha+5}) , \quad (3)$$

where the subscript $\alpha + \alpha'$ is meant to be taken modulo 6.

In the Boltzmann approach, the integer occupation numbers of the single-site velocity states are replaced by corresponding mean population values (probabilities), $f_\alpha = \langle s_\alpha \rangle$, which are real numbers. Furthermore, one considers the evolution not of individual particles but of the whole statistical ensemble of trajectories by performing an exact enumeration of possibilities. The dynamical equation, also called the lattice Bolzmann equation, is simply Eq. (2) where we replace the occupation state by its average value. This approximation is allowed because there is no correlation between particles arriving at a node. The corresponding kinetic equation is then

$$f_\alpha(t + 1, \vec{r} + \vec{c_\alpha}) = f_\alpha(t, \vec{r}) + \mathcal{C}_\alpha(\{f_\alpha\}). \quad (4)$$

Whenever a collision can lead to two possible outcomes each of the two is assigned a probability of $1/2$.

In most implementations [13,28] a linearized version

of Eq. (4) is adopted. In the linearization approximation, a small perturbation from the uniform solution is considered to contribute to the kinetic equation only to lowest order. Here we keep the full nonlinear version of the equation. We note that, with a proper handling of the algebra of the collision term, the nonlinear problem is still easily handled numerically so there is no technical need to introduce approximations.

Extra care is needed when the maximum number of rest particles n_0 is larger than 1. Consider a situation where the actual number of rest particles at a site is k_0, which is assumed to be less than n_0. Thus two kinds of collisions are possible—one kind involves a rest particle and the other one does not. We divide the 128 distinct Boolean configurations (0 or 1 particle at rest) into pairs—a configuration with and without a rest particle. Special attention has to be given to pairs which involve a change in the number of rest particles after a collision. As an illustration consider a situation, where there are two possible outcomes—one with k_0 rest particles and the other with $k_0 + 1$ particles. The former may correspond to a collision with a rest particle present as a passive spectator and the latter to an event involving no rest particles before the collision but with a rest particle after the collision. Following Gunstensen and Rothman [29], we choose the corresponding weights to be proportional to

$$\begin{pmatrix} n_0 \\ k_0 \end{pmatrix}$$

and

$$\begin{pmatrix} n_0 \\ k_0 + 1 \end{pmatrix},$$

respectively. If k_0 is noninteger the factorials in the combinatorials are replaced by Γ functions. This does not change the form of the kinetic equations and allows one to generalize the CA to contain several rest particles at a site.

The freedom in the choice of n_0 can be used to make the system Galilean invariant, i.e., to give the right coefficient to the convective (nonlinear) term in the Navier-Stokes equation. For this purpose n_0 has to satisfy the condition [13]

$$n_0 + 6 = 12\frac{1-\rho}{1-2\rho}. \tag{5}$$

When this condition is fulfilled, the BCA leads to the true Navier-Stokes equation.

In order to check the conditions at which our BCA becomes Galilean invariant, we have used the "shear wave test" [29]. In a BCA of size $N \times M$ an initial flow field is generated such that the center of mass velocity of the particles has a transverse shear wave $v_y = u \sin 2\pi x/N$ which moves horizontally with a velocity v_{sw}. Both v and u are small and the reduced density is fixed at the value of $1/3$. After 1000 time steps we compare the velocity of the flow v_{flow}, i.e., the velocity of the center of mass of the particles, and the measured velocity of the crest

of the shear wave, for different values of the maximum number of rest particles, n_0. In Fig. 1 we plot the velocity ratio (v_{flow}/v_{sw}) versus n_0 and we observe that the Galilean invariance sets in $(v_{flow}/v_{sw} = 1)$ for $n_0 = 18$ as predicted by Eq. (5).

The presence of Galilean invariance is especially important in two-fluid flows. Without it the vortex advection velocity does not match the interfacial velocity [13].

To complete the definition of a CA system, a choice of boundary conditions (typically periodic if there are no walls and bounce back reflection in the presence of no-slip walls) and a set of forcing rules which induce flows in the presence of pressure gradients or bulk forces have to be specified. Implementing the forcing rules is much easier for BCA than for the Boolean CA since they involve shift of the occupational probabilities, as explained in our previous papers [18,19].

The initial conditions depend on the flow we are interested in, but for a given reduced density ρ we usually set $f_\alpha = \rho$, $\alpha = 1, \ldots, 6$, and $f_0 = \rho n_0$. Throughout this paper we shall work with the Galilean invariant choice of reduced density ρ equal to $1/3$ and $n_0 = 18$. The corresponding density of state is then 8.

The dynamical viscosity η can be determined from the parabolic velocity profile in a planar Poiseuille flow [27]. In this case the pressure gradient is obtained by shifting probabilities f_α by a tiny amount in the flow direction ($+\epsilon$ in 2 and 6, and $-\epsilon$ in directions 3 and 5 if the net flow is parallel to the first direction). For $\rho = 1/3$ we get [19] $\eta = 1.46$ (we work in units in which the mass of a particle, its velocity, and the lattice constant are all unity). We have obtained the same value of η by generating a velocity fluctuation and then studying its relaxation [30]. This method also allows us to measure the sound velocity c_s. For a CA composed of particles of the same mass with n_0 states at rest the square of the sound velocity is given by [30] $c_s^2 = n_m / d(n_0 + n_m)$ where n_m is the number of moving states and d the spatial dimension. For a reduced density of $1/3$, $n_0 = 18$, and $n_m = 6$ the sound velocity should then be equal to $c_s = 1/\sqrt{8}$. This is indeed what we found, within 2%, using a system of size 256×32.
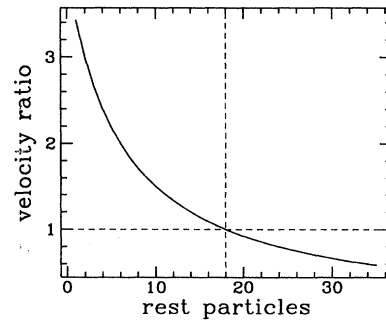

FIG. 1. Plot of the velocity ratio (velocity of moving particles v_{flow} divided by the shear wave velocity v_{sw}) versus the number of rest particles. The reduced density in each cell is $1/3$. The dashed lines show that Galilean invariance is restored, $v_{flow}/v_{sw} = 1$, for 18 rest particles as expected.

III. TWO-FLUID LATTICE BOLTZMANN AUTOMATON

We now generalize the BCA system defined in the preceding section to the two-fluid case. To this end we introduce particles of two colors. The state densities corresponding to the two colors will be denoted by r_α and b_α, for "red" and "blue," respectively, such that $f_\alpha = r_\alpha + b_\alpha$. The propagation step is applied to each color independently. The collision rules are basically color insensitive, i.e., they involve the total densities f_α, but after applying them the color content in the states is redistributed so that particles of opposite color effectively repel and particles having the same color attract.

This color sensitive interaction generates surface tension at an interface between the two colors. One way to introduce the immiscibility was proposed by Rothman and Keller [5] for a Boolean CA. They chose the after-collision color content in such a way that the color gradient times the net blue momentum minus the net red momentum was maximized. In this way the color redistribution flow is mostly in the direction of the color gradient. A generalized method was used for a BCA [13]. The procedure consists of two steps. The first step generates a perturbation in f_α proportional to a local color gradient—we find that the size of the perturbation controls the surface tension. The second step follows the Rothman and Keller paper [5] and consists of redistributing the color content of f_α to satisfy the color-color propensities. Both steps conserve the total color densities and total momentum at each site. Our approach is a modification of their method. We use the first step unchanged, but we propose a different way to realize the redistribution of color content. This way of color redistribution after the collision allows for interfaces of essentially arbitrary thickness.

To proceed we calculate the color gradient vector $\vec{g}$ at each node. Following Ref. [5] this vector can be defined as

$$\vec{g}(\vec{r}) = \sum_\alpha \vec{c_\alpha} \left(R_\alpha(\vec{r}) - B_\alpha(\vec{r}) \right) , \tag{6}$$

where R_α and B_α are the red and blue total densities on the neighbor site in the direction α, i.e., $R_\alpha = \sum_{\alpha'} r_{\alpha'}(\vec{r} + \vec{c_\alpha})$ and $B_\alpha = \sum_{\alpha'} b_{\alpha'}(\vec{r} + \vec{c_\alpha})$. We then increase the total (red+blue) state density in the direction collinear to the color gradient, and decrease the total density in all other directions. A smooth way to do this is given by

$$f'_\alpha = f_\alpha + \beta_1 |\vec{g}| \cos 2\phi_\alpha , \tag{7}$$

where ϕ_α is the angle between the color gradient (which need not coincide with any lattice direction) and the direction corresponding to state α. The parameter β_1, typically of order 0.001, allows us to choose a given value of the surface tension. The occupation of the rest state is not affected in this step.

Overall, the presence of the surface tension means that particles arriving close to an interface have a high probability of being sent backwards—normal to the interface.

The second step, of recoloration, has been designed in Refs. [5] and [13] so that the scalar product of the color gradient with the color momentum is maximized. This, however, leads to problems since the resulting interface has essentially no thickness and is unstable. Note that if n_0 is large the particles at rest make a powerful bank of color (for $\rho = 1/3$ and $n_0 = 18$, the total density in the six moving states is 2 on average, whereas there are of order six particles at rest); most of the interface nodes will have three moving states fully occupied by red particles and three states by blue ones. Only the rest state will contain both colors. On crossing the interface, there is typically only one node containing two different colors. All nodes away from the interface are essentially monochromatic. This case would correspond to a zero thickness interface since the color jump takes place over a single node. Such an abrupt interface would be extremely sensitive to its orientation with respect to the lattice. This would lead to nonphysical features such as faceted bubbles of one color, spatially anisotropic surface tension, etc. A way to attenuate these spurious flows is to spread them out over a wider interface. This can be alleviated by introducing a new color redistribution on each site proposed below.

In the second step we redistribute the color in such a way that the red minus blue density along the αth direction depends continuously on the angle ϕ_α between the αth axis and the color gradient. In addition to the conservation of the total red and blue colors on a site we also demand that $f_\alpha = r_\alpha + b_\alpha$. This leads us to the following equations:

$$r'_\alpha = \frac{R_t}{R_t + B_t} f'_\alpha + \beta_2 \frac{R_t B_t}{(R_t + B_t)^2} \cos \phi_\alpha ,$$

$$b'_\alpha = \frac{B_t}{R_t + B_t} f'_\alpha - \beta_2 \frac{R_t B_t}{(R_t + B_t)^2} \cos \phi_\alpha , \tag{8}$$
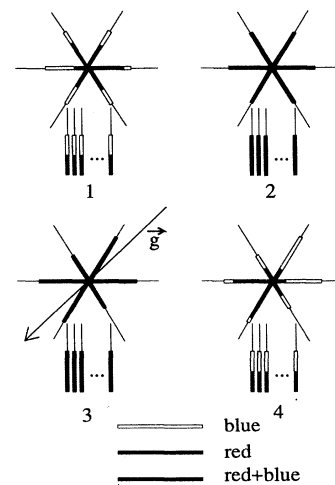
for the moving states and

FIG. 2. Example of color redistribution. (1) State of the cell just after the propagation step, (2) the collision operator is applied in a color insensitive way, (3) the directions close to the color gradient vector $\vec{g}$ have their density increased, and (4) the color redistribution.

$$r_0' = \frac{R_t}{R_t + B_t} f_0' ,$$

$$b_0' = \frac{B_t}{R_t + B_t} f_0' , \qquad (9)$$

for the states at rest. Here, β_2 (typically of order 0.2) affects the thickness of the interface and R_t and B_t are the total numbers of red and blue particles at the node being considered. An example of the color redistribution is shown in Fig. 2. In the next section we discuss the physical relevance of the two parameters β_1 and β_2.

IV. INTERFACIAL PROPERTIES

Let us first set β_1 and β_2 both equal to zero: the surface tension vanishes, the fluids become miscible, and the interface spreads because of molecular diffusion. This is shown in Fig. 3 where the density profiles at 1000 and 10 000 time steps after setting up the initial red-blue interface are plotted. The color density profiles are well represented by error functions which allows us to measure the molecular diffusion constant. We find $D = 0.25 \pm 0.05$.

A two-phase system tends to minimize its interfacial energy, i.e., to minimize its interface length. This is indeed happening in our BCA as illustrated in Fig. 4. Here, an initial interface is prepared as a square and then we observe how it undergoes a shape transformation during a 1000-step long evolution of the automaton ($\beta_1 = 0.002$ and $\beta_2 = 0.2$). The final interface is circular in shape. Its radius can be determined from the position of the total density dip. Figure 5 shows the effective radius of the circular blob as a function of the angular direction. The average value of the radius here is equal to 30. The superimposed fluctuations are seen to be tiny ($\sim 0.1/30$) which demonstrates that our rules generate a surface tension which is nearly isotropic.

To determine the interface thickness δx, we have performed a simulation on a 64×32 lattice with periodic boundary conditions along the interface where half of

FIG. 4. Immiscibility: an initially square blob of blue liquid in a red sea becomes circular in less than 1000 time steps.

the lattice is filled with particles of one color, and the remaining half with the other color. Along the interface the boundary conditions are periodic. In the other direction there are bounce back boundary conditions on the walls containing the fluid. Figure 6 shows a plot of the color density profile along a line normal to the interface. This figure shows that the stable interface extends now over several nodes of the lattice. From the tangent hyperbolic shape of these profiles we can measure the interface thickness. We defined it as the width corresponding to a relative concentration variation between 0.25 and 0.75 (color density between 2 and 6). We find that δx is essentially independent of β_1 but is controlled by β_2 (Fig. 7); the larger the value of β_2 the smaller is the δx.

In Fig. 8 the total (red + blue) density profile along a line which crosses the interface is plotted. It shows a depletion in the density at the center of the interface. This effect is similar to what is observed at interfaces of real fluids [13] and its strength is proportional to β_1.

An easy way to measure the surface tension coefficient is to check Laplace's law for a drop of fluid surrounded by another fluid. In two dimensions Laplace's law states

$$\delta p = \frac{\gamma}{l} , \qquad (10)$$

where δp is the pressure difference between the inner and outer sides of the drop of radius l (measured to the mid-
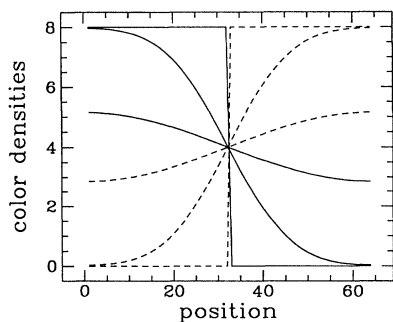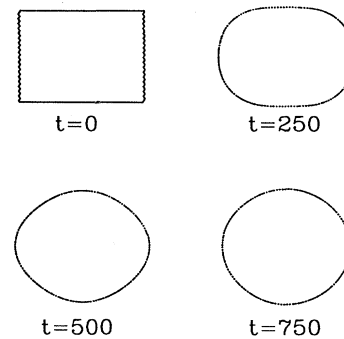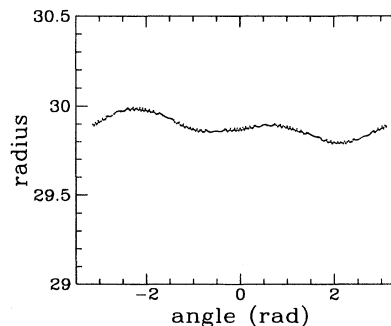

FIG. 3. The situation corresponding to complete miscibility: $\beta_1 = 0$ and $\beta_2 = 0$. An initially sharp interface ($t = 0$) vanishes due to "molecular" diffusion. The red and blue state densities are plotted versus position (lattice units) for time steps 1000 and 10 000.

FIG. 5. Radius of the circular blob of Fig. 4 versus the polar angle $(-\pi, \pi)$. The fluctuations (~ 0.1) in the effective radius are small compared to the average radius (30).
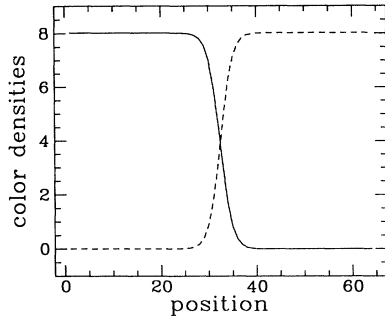
FIG. 6. Red (solid line) and blue (dashed line) state densities are plotted on a line crossing an interface. The values of our control parameters are $\beta_1 = 0.0015$ and $\beta_2 = 0.15$.

FIG. 8. Plot of the total state density (red+blue) on a line crossing an interface. $\beta_1 = 0.0015$ and $\beta_2 = 0.15$. The interface region shows a decrease of the total density, accounting for the surface tension.

dle of the interface). In a CA, what one can determine directly is not the pressure difference but the density difference $\delta\rho$ across the interface. The two quantities are related through the equation $p = \rho c_s^2$ where c_s is the sound velocity, which was discussed in Sec. II. The red and blue densities needed to determine the pressure difference are measured sufficiently far from the interface. In practice, we determined densities on those sites which were at least 98% monochromatic.

We studied Laplace's law in a BCA of size 100×120 and determined the surface tension coefficient from the plot of δp versus the inverse radius l of the stable circular blob. This is shown in Fig. 9. We note that each curve intersects the pressure axis close to the origin. Laplace's law is indeed satisfied. Even though in our BCA the interface properties are controlled by two parameters, β_1 and β_2, it is only β_1 which really controls γ. For instance, for $\beta_1 = 0.001$ we get $\gamma = 0.184 \pm 0.001$ and 0.182 ± 0.001 for β_2 equal to 0.2 and 0.25, respectively. The dependence on β_1 is basically linear.

In order to reduce the interface control to one parameter we can set $\beta_2 = 100\,\beta_1$ and vary both coefficients in proportion to each other. Figure 10 shows the surface tension vs β_1 ($\beta_1 = 0.01\beta_2$). We find that the dependence is basically linear. The surface tension corresponding to $\beta_1 = 0.002$ is $\gamma = 0.37 \pm 0.01$. We note that the range of the values of γ shown in the figure covers half a decade be-

tween 0.1 and 0.55. This kind of freedom in the choice of γ is hardly available with a Boolean CA. Studying lower values of γ requires considering much larger system sizes because the interface width becomes large—larger than 40 lattice constants.

When β_1 and β_2 are varied independently, we find that the coefficient of the surface tension depends on β_1 linearly whereas it is essentially independent of β_2. Thus, while the coefficient of surface tension is controlled by β_1, the interface thickness appears to be controlled by β_2: it is proportional to its inverse.

The two-parameter control of the interface is reminiscent of the classical approach to the interfacial properties of nonuniform systems [31,32]. An example is the interface in the van der Waals fluid: the continuous variable is the density and the two equilibrium states are the low and high density phases corresponding to gas and liquid, respectively. In our two-color BCA, the analogous equilibrium states are the fully red and fully blue liquids and the continuous variable is the relative density of one
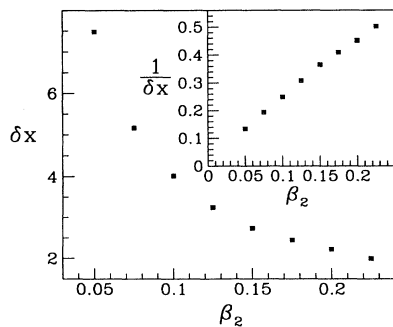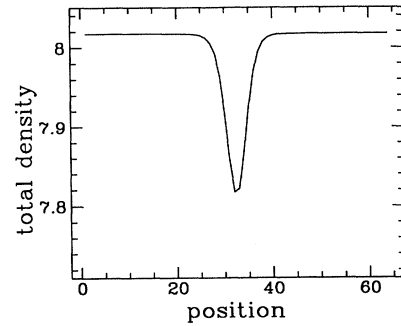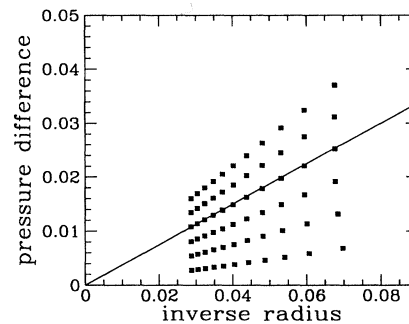

FIG. 7. Interface thickness δx in lattice units, versus the control parameter β_2. The inset shows that the inverse thickness depends on β_2 in a linear fashion.

FIG. 9. For several bubble radii and six values of β_1 ($\beta_1 = 0.0005, 0.001, ..., 0.003$ and $\beta_2 = 100\beta_1$), we have measured the pressure difference between the inside and the outside of the bubble. For each value of β_1, a straight line through the points crosses the axis close to the origin, as shown for $\beta_1 = 0.002$. The slope of this line is the surface tension (CA units).
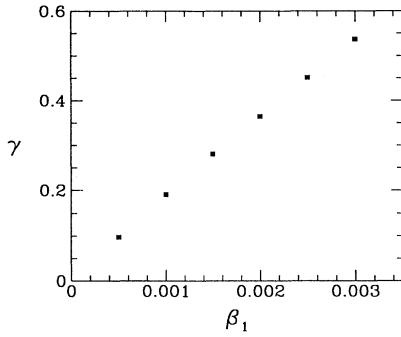
FIG. 10. The surface tension (CA units), as measured from Fig. 9, versus β_1.

color. The free energy of a nonuniform system depends on the square of the density gradient through the interface. In the simplest model the interfacial tension can be written as

$$\gamma = \int_{-\infty}^{+\infty} S \left(\frac{\partial \rho}{\partial x}\right)^2 dx , \qquad (11)$$

where x is a direction across the interface and S the stiffness (assumed to be constant here) of the interface. Consider a situation in which the two phases correspond to minima of a double-well potential and that the energy barrier is equal to W. The interface properties are then governed by the parameters S and W. The density variation across the equilibrium interface is described by $\rho \sim \tanh x/\delta x$. The interface thickness and γ are then given by

$$\delta x \sim \sqrt{S/W} , \qquad (12)$$

$$\gamma \sim \sqrt{SW} , \qquad (13)$$

respectively.

In order to relate β_1 and β_2 to S and W, we have computed the integral of the density gradient $\left(\frac{\partial \rho}{\partial x}\right)^2$ across the interface (which is equal to γ/S) numerically. We find that γ/S essentially does not depend on β_1 and is almost linear in β_2 ($\gamma/S \sim \beta_2$). From Fig. 10 we also have $\gamma \sim \beta_1$. Combining these two, we conclude that $S \sim \beta_1/\beta_2$. Note also from Eq. (13) that $W \sim \beta_1\beta_2$. This means that $\delta x \sim 1/\beta_2$ which is precisely what has been demonstrated in the inset of Fig. 7. Thus our simple understanding of the interface in terms of S and W can account for the observed dependencies of γ and δx on the two parameters β_1 and β_2.

V. DROP DEFORMATION

In order to perform further tests on our BCA we consider small deformations in the shape of an initially circular drop placed in a slow shear flow (a fast shear would lead to drop rupture [33]). The theoretical and experimental literature on drop deformation is quite substantial [34,35]. Figure 11 shows the stationary shape of a drop which initially had a radius b of 20. The shape can be
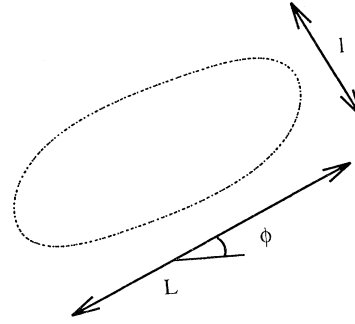

FIG. 11. Sketch of the shape of a drop in a linear shear flow.

characterized by the tilt angle Φ and the deformation ratio $E = \frac{L-l}{L+l}$ where L and l are the length and the width of the deformed drop (Fig. 11).

The applied shear rate is $G = U_0/H$ where $U_0 = 0.042$ is the velocity at the horizontal walls. The flow direction is from left to right at the top wall and the opposite at the bottom wall. The moving walls are separated by a distance $2H = 64\sqrt{3}/2$ across the system. The measured drop deformation is almost linear in U_0. Furthermore, the larger the U_0, the larger the tilt angle Φ with the horizontal direction. The shape of the drop is determined by a competition between shear, which favors a slender drop, and interfacial tension, which favors a circular shape. From dimensional arguments [33], the drop deformation depends on the reduced shear rate $k = Gb\eta/\gamma$ (η is the single-fluid viscosity—which is the same for the two fluids, η=1.46) and the characteristic time scale of the phenomenon is $\tau = b\eta/\gamma$. For $G\tau \gg 1$, the drop elongates and rotates wobbling around its asymptotic equilibrium direction, whereas for $G\tau \ll 1$ the drop elongates and rotates in an overdamped manner. The complete calculation in three dimensions [34,35] (in agreement with the experiment [33,35]) yields an equilibrium shape characterized by

$$E \simeq k , \qquad (14)$$

$$\Phi = \frac{\pi}{4} - \frac{1}{2}\arctan k . \qquad (15)$$
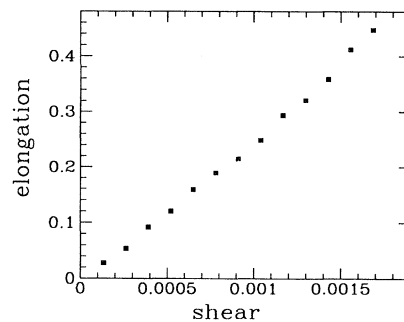
In Fig. 12 we plot the deformation ratio E versus the

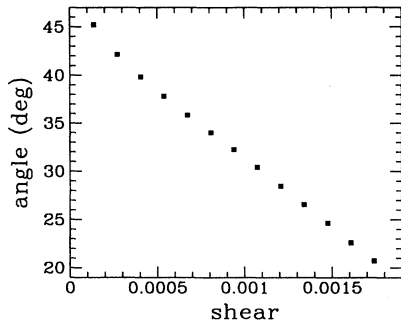FIG. 12. The elongation E of the bubble is plotted versus the shear rate G (inverse time step units).

FIG. 13. The tilt angle is plotted versus the strength of the shear rate (CA units). The first points (shear < 0.0005) are not accurate since the blob is very close to a circle. But if we were to plot the points corresponding to larger shear, the extrapolated line would cross the vertical axis at an angle of 45° as expected.

shear G. As expected the elongation increases linearly with the shear rate, and the slope crosses the axis very close to the origin. Figure 13 shows the plot of the tilt angle versus the reduced shear. For small shear the tilt angle is close to 45° (note that in this limit the bubble is nearly a circle, and the tilt angle is not measured accurately—its value is overestimated). As the reduced shear rate k is small and $\arctan k \simeq k$, the plot is basically linear. The regime with larger k is difficult to reach because of the rupture taking place first. Our measurements in 2D (Figs. 12 and 13) lead to $E \simeq 3k$ and $\Phi \simeq \frac{\pi}{4} - 3k$ whereas the 3D calculations [33,34], lead to Eqs. (14) and (15). Hence we get the main features but not the same prefactors.

VI. WETTING PROPERTIES

We now consider problems which, like wetting, involve interactions of particles with a wall. The usual way of creating a wall with no-slip boundary conditions is to impose bounce back reflection on the particles arriving at a node adjacent to the wall. In order to attribute specific wetting properties to the wall we should assign to it a particular color content [5]. This will affect the color gradients on the nodes adjacent to the walls. The BCA allows one to set the color content on the wall sites in arbitrary relative proportions of red to blue.

A bubble of one color in contact with a wall of the same color should spread on the wall completely. On the other hand, if the wall is of the opposite color, the blob should be repelled, which corresponds to a perfectly nonwetting case. Intermediate situations should lead to a partial wetting. Figure 14 shows the dewetting of a semi-circular drop placed on a perfectly nonwetting wall (i.e., the color assigned to the wall is opposite to the color of the drop). The dewetting process in this BCA is very slow. It takes nearly 9000 time steps to complete the dewetting of a drop of radius 40. In the opposite case of complete wetting, even more time steps are needed; the process is eventually affected by the side walls that the drop reaches on spreading.
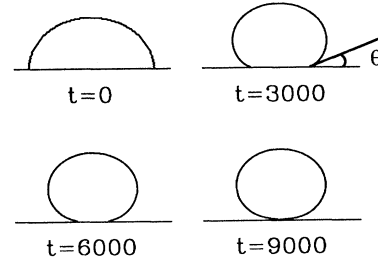

FIG. 14. Dewetting of a drop placed on a wall surface of opposite color, shown at various times of the evolution.

In Fig. 15 we plot the contact angle θ versus the wall color ratio $[R_t/(R_t + B_t)]$. The data points indicated by the triangles and crosses are the angles obtained after 6000 and 18 000 time steps of evolution, respectively, starting from a semicircular drop which corresponds to a 90° initial contact angle. The shape of the 6000-step line shows clearly that the system is still in the process of reaching equilibrium. After 18 000 steps most of the wetting situations are fully equilibrated. Further evolution till 60 000 time steps (squares) shows that the complete wetting situation is affected by the presence of side walls. We notice that there are no preferential contact angles parallel or perpendicular to the lattice, which is consistent with the isotropic surface tension produced by our BCA. We have tested other rules in which recoloring was done differently, as described in Sec. III, but these lead to quantized wetting angles. In our case the contact angle varies basically linearly with the relative color content of the wall.

VII. EFFECT OF GRAVITY

The effect of gravity can be easily mimicked in a CA by increasing the densities in the direction of the gravitational force by a small amount. Consider the situation in which the gravitational force acts perpendicular to the line set by directions 1 and 4. Suppose the blue fluid is of lower density and the red fluid of higher density. In this two-liquid case only the density difference between the fluids is relevant. Thus we modify the output of the
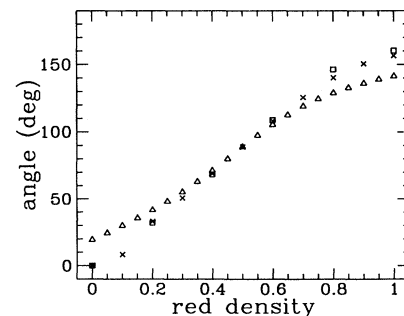

FIG. 15. Plot of the contact angle versus the relative color content of the wall. Triangles, crosses, and squares show the situation after 6000, 18 000, and 60 000 time steps, respectively.
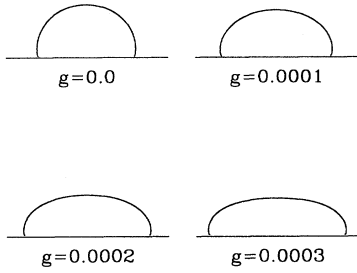
FIG. 16. Blob profiles are shown for several values of the gravitational field (CA units).

collision step by sending more particles in the upper directions (states 2 and 3) if the site is mainly blue, and in the opposite directions (states 5 and 6) for red sites. We apply

$$f'_{2,3} = f_{2,3} + \rho \frac{R_t - B_t}{R_t + B_t} g \ ,$$

$$f'_{5,6} = f_{5,6} - \rho \frac{R_t - B_t}{R_t + B_t} g \ , \qquad (16)$$

where g is the gravity control parameter. In Fig. 16, we show that on increasing g from 0 to 0.0003 the profile of an initial half-circular drop becomes flatter and flatter.

It is easy to characterize the effect of gravity by measuring the increase of pressure along a vertical column of a one-phase liquid, and then by applying

$$\Delta p = \rho_s \, g_{ef} \, h \ , \qquad (17)$$

where g_{ef} is the effective gravity of the system, and ρ_s is the effective density of the BCA $[\rho_s = (6 + N_0)\, \rho\, 2/\sqrt{3}]$. For a reduced density of $1/3$, $n_0 = 18$, and $g = 0.0003$, we have obtained an effective gravity of $g_{ef} = 2.93 \times 10^{-5}$. The relation between these two parameters is linear.

A simple variational approach shows [36] that in the case of a two-dimensional large drop on a flat surface, the distance between the equatorial plane and the apex h obeys the relation

$$\gamma = \frac{\Delta \rho \, g_{ef} \, h^2}{2} \ . \qquad (18)$$

With a surface tension of $\gamma = 0.28$, this equation yields $h = 32.1$. We have performed a BCA simulation for various drop sizes leading to h values of 32 ± 3. Considering the small size of the system ($256 \times 64\sqrt{3}/2$), the agreement between these values is rather good.

Another interesting problem is to check if gravity affects contact angles. Figure 16 suggests that even though the shape of the drop is drastically affected the contact angle remains unchanged. Figure 17 shows the contact angles for various partial wetting cases (the drop is red and color on the wall varies the red content from 30% to 70%), for the effective gravity g_{ef} equal to 0, 0.982×10^{-5}, and 1.97×10^{-5} (corresponding to $g = 0$, 0.0001, and 0.0002 respectively). The contact angles are seen not to be affected for small values of G. The slight differences are mostly due to the difficulty in measuring a contact angle on a very flattened drop.
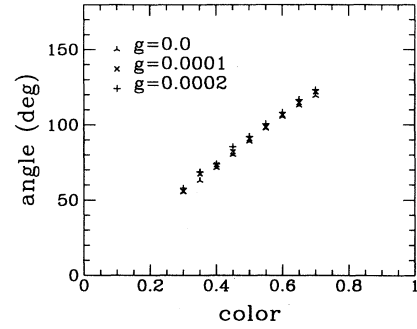

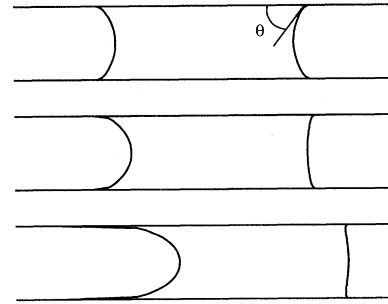FIG. 17. Plots of the contact angle versus the relative color content for various gravity fields.

FIG. 18. A blob within two partially wetting walls with three different velocities $V = 0.489 \times 10^{-3}$, 4.58×10^{-3}, and 9.5×10^{-3} increasing from top to bottom (CA units).
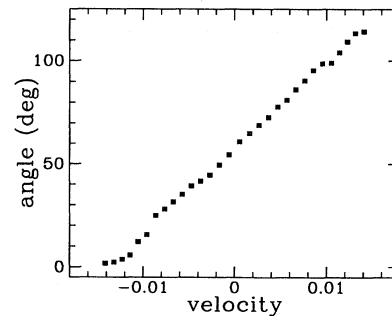

FIG. 19. The dynamical contact angle shown as a function of velocity (CA units). This is a partially wetting case: the static contact angle is $45°$.

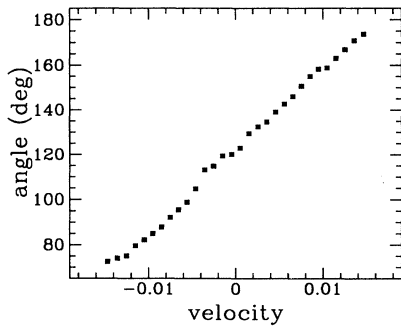FIG. 20. Same as Fig. 19 but for the partially nonwetting case: the static contact angle is 135°.

VIII. WETTING DYNAMICS

We now ask what happens to the contact angle when there is a net flow through the system and, more specifically, how the apparent contact angle depends on the flow rate.

In order to measure the dynamical contact angle θ, we perform the following simulation. A partially wetting red bubble is flushed between two walls by inducing a flow from left to right in a channel (Fig. 18). The velocity of displacement of the bubble is, from top to bottom, $V = 0.489 \times 10^{-3}$, 4.58×10^{-3}, and 9.5×10^{-3}. As expected, the dynamical contact angle increases with the capillary number Ca$= \mu V/\gamma$, which is proportional to the flow velocity.

In Fig. 19, we have plotted the dynamical contact angle versus the velocity in the case of a partially wetting liquid. Figure 20 is the same as Fig. 19, but it refers to the case of a partially nonwetting liquid. Even though these two plots look physically reasonable, it is not possible to check whether either Tanner's law [21] or predictions of the more general theory of Cox [20] are fulfilled. In fact Tanner's law, which relates velocity and contact angle through $\theta \sim \text{Ca}^{1/3}$ for low θ values, holds

only for a completely wetting liquid-gas interface. Very small contact angles are difficult to study to a high precision (the drop can break and the innate lattice structure does not allow for precise measurement). Our results are qualitatively consistent with those obtained theoretically and experimentally by Fermigier and Jenffer [37].

IX. CONCLUSIONS

We have designed a two-fluid nonlinear lattice Boltzmann automaton which satisfies Galilean invariance. The recoloration rules in collisions allow for a convenient way to introduce and control the surface tension [38].

The molecular diffusion coefficient is measured in the miscible case. Simulations of drop deformation in a linear shear flow are in qualitative agreement with theory.

The BCA allows a continuous control of the contact angle from complete wetting to complete nonwetting. The simulation of the deformation of a drop placed on a surface is in good quantitative agreement with theory. The dynamic contact angle depends on the flow rate. Application of this BCA to flows and spinodal decomposition in porous media is currently in progress.

ACKNOWLEDGMENTS

[1] U. Frisch, D. d'Humières, B. Hasslacher, P. Lallemand, Y. Pomeau, and J.-P. Rivet, Complex Syst. **1**, 649 (1987).

[2] *Cellular Automata and Modelling of Complex Physical Systems*, edited by P. Manneville, N. Boccara, G. Y. Vichniac, and R. Bideaux (Springer-Verlag, Berlin, 1989).

[3] U. Frisch, B. Hasslacher, and Y. Pomeau, Phys. Rev. Lett. **56**, 1505 (1986).

[4] D. d'Humières, P. Lallemand, and U. Frisch, Europhys. Lett. **B2**, 291 (1986).

[5] D. H. Rothman and J. M. Keller, J. Stat. Phys. **52**, 1119 (1988).

[6] M. Bonetti, A. Noullez, and J.-P. Boon, in *Discrete Kinetic Theory, Lattice Gas Dynamics, and Foundations of Hydrodynamics*, edited by R. Monaco (World Scientific, Singapore, 1989), p. 395.

[7] C. Apert and S. Zaleski, Phys. Rev. Lett. **64**, 1 (1990).

[8] A. J. C. Ladd, M. E. Colvin, and D. Frenkel, Phys. Rev.

Lett. **60**, 975 (1988).

[9] J. M. Vianney and A. Koelman, Phys. Rev. Lett. **64**, 1915 (1990).

[10] C. Baudet, J. P. Hulin, P. Lallemand, and D. d'Humières, Phys. Fluids A **1**, 507 (1989).

[11] D. Bernardin, O. E. Sero-Guillaume, and C. H. Sun, Physica D **40**, 169 (1991).

[12] G. R. McNamara and G. Zanetti, Phys. Rev. Lett. **61**, 2332 (1988).

[13] A. K. Gunstensen, D. H. Rothman, S. Zaleski, and G. Zanetti, Phys. Rev. A **43**, 4320 (1991), and references therein.

[14] S. Succi, R. Benzi, and F. Higuera, Physica D **47**, 219 (1991); R. Benzi, S. Succi, and M. Vergassola, Phys. Rep. **222**, 145 (1992).

[15] F. J. Alexander, S. Chen, and D. W. Grunau, Phys. Rev. B **48**, 634 (1993); D. W. Grunau, T. Lookman, S. Y. Chen, and A. S. Lepedes, Phys. Rev. Lett. **71**, 4198

(1993).

[16] Y. H. Qian, D. d'Humieres, and P. Lallemand, Europhys. Lett. **17**, 479 (1992); X. Shan and H. Chen, Phys. Rev. B **47**, 1815 (1993).

[17] J. M. Ottino, C. W. Leong, H. Rising, and P. D. Swanson, Nature **333**, 419 (1988); J. M. Ottino, Sci. Am. **260**, 56 (1989).

[18] M. Cieplak, U. D'Ortona, D. Salin, R. B. Rybka, and J. R. Banavar, Comp. Mater. Sci. **1**, 87 (1992).

[19] R. B. Rybka, M. Cieplak, U. D'Ortona, D. Salin, and J. R. Banavar, Phys. Rev. E **48**, 757 (1993).

[20] R. G. Cox, J. Fluid Mech. **186**, 169 (1986).

[21] P. G. de Gennes, Rev. Mod. Phys. **57**, 827 (1985).

[22] E. B. Dussan V, Annu. Rev. Fluid Mech. **11**, 371 (1979).

[23] J. x. Yang, J. Koplik, and J. R. Banavar, Phys. Rev. A **46**, 7738 (1992).

[24] J. Koplik, J. R. Banavar, and J. F. Willemsen, Phys. Fluids A **1**, 781 (1988).

[25] P. A. Thompson and M. O. Robbins, Phys. Rev. Lett. **63**, 766 (1989); M. Cieplak, E. Smith, and M. O. Robbins (unpublished).

[26] A. M. Cazabat, Contemp. Phys. **28**, 347 (1987).

[27] M. Hénon, Complex Syst. **1**, 763 (1987).

[28] F. J. Higuera, S. Succi, and R. Benzi, Europhys. Lett. **9**, 345 (1989).

[29] A. Gunstensen and D. Rothman, Physica D **47**, 53 (1991).

[30] D. d'Humière and P. Lallemand, Complex Syst. **1**, 599 (1987), and references therein.

[31] J. W. Cahn and J. E. Hilliard, J. Chem. Phys. **28**, 258 (1958).

[32] N. G. Van Kampen, Phys. Rev. **135**, A362 (1964).

[33] G. I. Taylor, Proc. R. Soc. London Ser. A **146**, 501 (1934).

[34] J. M. Rallison, Annu. Rev. Fluid Mech. **16**, 45 (1984), and references therein.

[35] A. Adamson, *Physical Chemistry of Surfaces* (John Wiley and Sons, New York, 1982).

[36] S. Torza, R. G. Cox, and S. G. Mason, J. Colloid Interface Sci. **38**, 395 (1972), and references therein.

[37] M. Fermigier and P. Jenffer, J. Colloid Interface Sci. **146**, 227 (1991).

[38] U. D'Ortona, D. Salin, M. Cieplak, and J. R. Banavar, Europhys. Lett. **28**, 317 (1994).